MISSOURI S&T

CENTER FOR TRANSPORTATION INFRASTRUCTURE AND SAFETY

Structural Health Monitoring and Remote Sensing of Transportation Infrastructure Using Embedded Frequency Selective Surfaces

by

PI Edward C. Kinzel[1], Co-PI Kristen M. Donnell[2], Co-PI K. Chandrashekhara[1]

[1] Department of Mechanical and Aerospace Engineering
[2]Department of Electrical and Computer Engineering
Missouri University of Science and Technology

A National University Transportation Center at Missouri University of Science and Technology

NUTC R365

Disclaimer

The contents of this report reflect the views of the author(s), who are responsible for the facts and the accuracy of information presented herein. This document is disseminated under the sponsorship of the Department of Transportation, University Transportation Centers Program and the Center for Transportation Infrastructure and Safety NUTC program at the Missouri University of Science and Technology, in the interest of information exchange. The U.S. Government and Center for Transportation Infrastructure and Safety assumes no liability for the contents or use thereof.

Technical Report Documentation Page

1. Report No.	2. Government Accession No.	3. Recipient's Catalog No.
NUTC R365		

4. Title and Subtitle	5. Report Date
Structural Health Monitoring and Remote Sensing of Transportation Infrastructure Using Embedded Frequency Selective Surfaces	July 2014
	6. Performing Organization Code

7. Author/s	8. Performing Organization Report No.
Edward C. Kinzel, Kristen M. Donnell, K. Chandrashekhara	Project # 00043736

9. Performing Organization Name and Address	10. Work Unit No. (TRAIS)
Center for Transportation Infrastructure and Safety/NUTC program Missouri University of Science and Technology 220 Engineering Research Lab Rolla, MO 65409	11. Contract or Grant No. DTRT06-G-0014

12. Sponsoring Organization Name and Address	13. Type of Report and Period Covered
U.S. Department of Transportation Research and Innovative Technology Administration 1200 New Jersey Avenue, SE Washington, DC 20590	Final
	14. Sponsoring Agency Code

15. Supplementary Notes

16. Abstract

The objective of this project was to investigate the use of Frequency Selective Surfaces (FSS) for structural health monitoring applications. Frequency Selective Surfaces (FSS) have long been used in the RF/microwave community to control scattering from surfaces. In our application, the scattering parameters of the FSS form a signature which is a function of the frequency, element size and spacing, as well as the local electromagnetic environment. These attributes can be related to engineering parameters of a transportation structure such as strain, temperature, moisture, and damage such as cracking or delamination. A key advantage of the FSS approach over other wireless sensors is that the FSS is completely passive, consisting only of conductive elements. This eliminates considerations related to integrating power/energy storage, as well as simplifying fabrication.

17. Key Words	18. Distribution Statement
words	No restrictions. This document is available to the public through the National Technical Information Service, Springfield, Virginia 22161.

19. Security Classification (of this report)	20. Security Classification (of this page)	21. No. Of Pages	22. Price
Structural health monitoring, microwave nondestructive testing, transportation infrastructure, and composites	unclassified	22	

Form DOT F 1700.7 (8-72)

NUTC/Structural Health Monitoring and Remote Sensing of Transportation Infrastructure Using Embedded Frequency Selective Surfaces – Final Report

PI Edward C. Kinzel[1], Co-PI Kristen M. Donnell[2], Co-PI K. Chandrashekhara[1]

[1] Department of Mechanical and Aerospace Engineering

[2]Department of Electrical and Computer Engineering

Missouri University of Science and Technology

Submitted to:

Dr. Kamal Khayat, Director

Center for Transportation Infrastructure and Safety,

A National University Transportation Center (NUTC)

Missouri University of Science and Technology

Introduction

1.1 Project Objective

The objective of this project was to investigate the use of Frequency Selective Surfaces (FSS) for structural health monitoring applications. Frequency Selective Surfaces (FSS) have long been used in the RF/microwave community to control scattering from surfaces. In our application, the scattering parameters of the FSS form a signature which is a function of the frequency, element size and spacing, as well as the local electromagnetic environment. These attributes can be related to engineering parameters of a transportation structure such as strain, temperature, moisture, and damage such as cracking or delamination. A key advantage of the FSS approach over other wireless sensors is that the FSS is completely passive, consisting only of conductive elements. This eliminates considerations related to integrating power/energy storage, as well as simplifying fabrication.

We study integrating a FSS with a structure (on the surface or embedded within the part). Our FSS allows measurement of the strain field but could by easily extended to other parameters of interest. This approach has potential for Structural Health Monitoring (SHM), for example remotely detecting the strain on a gusset plate or other parts of a bridge. An in-service component can be quickly and remotely interrogated for damage, initially using standard microwave network-analyzer/antennas. Additional localized inspection can be performed on an as-needed basis to determine more detailed information regarding local strain field (or other relevant parameters).

The remainder of the report is organized as follows. The introduction report reviews SHM and FSS. Section 2 presents an initial design for a FSS sensor created for the project is presented. This sensor design is analyzed and used to illustrate the potential of the process. Section 3 describes initial fabrication efforts. We investigated different patterning techniques including screen printing and using a stencil with an airbrush, however, for surface mounted sensors traditional PCB etching works. Section 4 describes initial testing of this sensor. Finally Section 5 concludes the report and provides suggestions for further research.

1.2 Structural Health Monitoring

Structural Health Monitoring (SHM) is the scientific process of damage detection and identification in engineering structures. In this context, damage is defined as changes in the system that adversely affects its current or future performance. The state of the system is determined by taking characteristic measurements and observing how they change over time. Damage-sensitive features may be extracted from these measurements to determine the integrity of the structure as it ages or after extreme events such as earthquakes or blast loading. Quantifying the existence, location, type, and extent of damage in addition to prediction of the future useful life-time of the structure is an important and active research area [1].

Many different damage detection methods have been proposed and implemented. These can generally be divided between local-based and global-based damage detection methods [2]. Local-based techniques detect damage such as cracks, yielding, or delamination by interrogating a structure over a finite area. This includes NDT techniques such as ultrasonic inspection and

thermography. Global-based damage detection refers to instrumenting a structure with a finite number of discrete sensors. These are commonly point sensors such as strain gauges or accelerometers. Since point sensors only directly interrogate a limited area, ascertaining the health of an entire structure generally involves additional testing or analysis; for example, inferring damage by observing changes in vibration properties. Damage alters the stiffness, density, or energy dissipation properties of the structure which will change its natural frequencies. Calibrated modal testing or baseline measurements (often aided with structural modeling, statistical analysis or unsupervised learning such as neural networks) are required to distinguish the damaged response from a healthy system [1]. Notwithstanding this effort, global SHM is currently used in bridges and is in the developmental stages for aerospace structures as well as other systems where failure may be potentially catastrophic in terms of loss-of-life or economic expense such as wind turbines.

SHM requires sensors to resolve the parameter being related to the health of the system. These sensors can either be bonded to the surface of an existing structure or embedded during manufacturing to form a smart structure. Using wireless sensors has significant advantages when monitoring a large structure such as a bridge or a structure with moving parts. Wired sensors require long wires and hard connections in addition to the use of equipment such as slip collars which complicate instillations. Wireless motes and active RFID (Radio Frequency Identification) techniques can be implemented for applications where hard connections are not feasible [2], but this is at the expense of power requirements which must be resolved by storing energy on board, harvesting energy locally [3] or transferring energy wirelessly, complicating the sensor design and making embedding more difficult.

Nondestructive Testing (NDT) techniques such as microwave, ultrasound, and thermography are also widely used to evaluate the health of structures. These NDT approaches can be accomplished without additional sensors and have lower requirements for structural modeling or statistical baselining. This is because they are local methods and interrogate an area of the structure rather than at discrete points. NDT techniques such as thermography and ultrasound are good at identifying and locating damage, including sub-surface damage, but damage quantification in the field often requires trained personnel. In addition, the operator often must have knowledge of the potential damage regions to prioritize inspection of a complete structure. Similarly, measuring parameters such as strain in an in-service environment prior to failure can be very challenging. This can be improved by employing NDT techniques with embedded sensors.

Both local and global SHM are particularly important in composite structures. Composites have excellent mechanical properties (e.g., strength, stiffness, and stiffness-to-density ratio), long-term durability, and fabrication flexibility. This has led to their widespread use in applications including aerospace, maritime, automotive, infrastructure, and energy. However, composites are susceptible to damage and have different failure mechanisms than conventional materials. Failures can occur as a result of manufacturing defects such as voids or may occur in-service due to impact or fatigue damage resulting in delaminations, disbonds, and cracks. Often the damage or defects are internal and can be difficult or impossible to observe visually. This is particularly true for low-energy impacts that produce minimal surface damage but lead to cracks that subsequently initiate failure.

The engineered layer-by-layer fabrication of composites lends itself well to the formation of a smart structure by including embedded sensors. Fiber Bragg grating sensors are often used for composite applications because they can survive the composite processing temperatures and allow in-situ characterization of the fabrication process in addition to in-situ monitoring of the structure in service [4]. However, feature-extraction can be complicated by the fact that composites are heterogeneous and anisotropic; making the behavior of composites more difficult to model than conventional materials (e.g. the resonant frequency is more sensitive to temperature than to small cracks).

1.3 Frequency Selective Surfaces

Frequency Selective Surfaces have been studied intensively since the 1960s for use as spatial filters. They provide an important function in radome design, where FSS's are used to reduce the Radar Cross Section (RCS) of antennas outside their operational band [5]. They have also been used as dichroic elements in antenna reflectors and microwave polarizers. Because of their technological significance, both analytical and numerical techniques have been developed for their analysis and design. Furthermore, in the past decade they have been scaled down to terahertz (THz), infrared, and visible wavelengths where they have been rebranded as "metamaterials" or "metasurfaces" [6]. In this document we still use the term FSS to denote the specific class of devices we are proposing to avoid confusion with techniques extracting effective permittivity/permeability [7].

The key functionality of an FSS is the ability to control the electromagnetic response (reflection and transmission properties) from a structure. Designing an FSS as a resonant structure allows us to design one or more sharp changes in the response at a prescribed frequency (or frequencies). Since these spectral features are strongly dependent on the geometry of the FSS as well as the local material environment, changes in these parameters will impact the electromagnetic response, herein referred to as the FSS signature. This dependency is incorporated into the design of the FSS, allowing for optimization of the FSS per specific applications. There are a wide variety of FSS elements that have been studied, some of which are shown below in Fig. 2 [5].

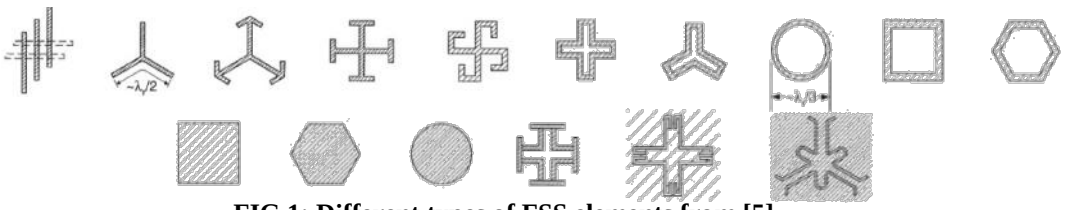

FIG 1: Different types of FSS elements from [5].

The application of FSS to strain measurement has only recently been considered in literature. The last five years have seen several groups using FSS to telemetrically measure strain at both microwave (X-band) [8-12] and THz/IR frequencies [13]. This is similar to the inverse problem of tuning an FSS in the IR or visible bands by straining it [14-15]. Many of these designs include a Split-Ring Resonator (SRR) as the FSS element [8-10], although half-wave dipole-based designs have also been implemented [12-13].

There are several factors that affect the choice of operating frequency. The feature sizes of an FSS element scale according to the resonant wavelength, λ_0. Generally, the length of the element is selected to be on the order of $\lambda_0/2$, although the features may be much smaller. The

periodicity, p (illustrated below in Fig. 3), should be less than 0.4 λ_0 to prevent diffraction and undesirable changes in the FSS signature with respect to angle of incidence [5] (an important consideration for practical application). Related to this, the minimum feature size also dictates the possible fabrication technology. The FSS needs to be cost-effective if it is to be deployed over a large area. Generally, using thick-film, rather than thin-film, processing will result in a much lower-cost manufacturing, limiting the minimum feature size to greater than 75 μm [16].

The choice of frequency is also determined by the material system. While this is less critical for a surface mounted FSS, electromagnetic energy must penetrate the material for an embedded approach. Many materials have vibrational/rotational absorption bands at THz and IR frequencies but are transparent to microwaves. The spatial resolution is determined by the size of the interrogating beam on the FSS and will also be quantized by the size of the FSS elements. Frequencies in the microwave-to-millimeter wave range will likely meet these requirements. Further, the choice of operating frequency also affects the cost of the test equipment. Vector Network Analyzers (VNA) and Spectrum Analyzers (SA) are widely available at microwave frequencies at reasonable cost.

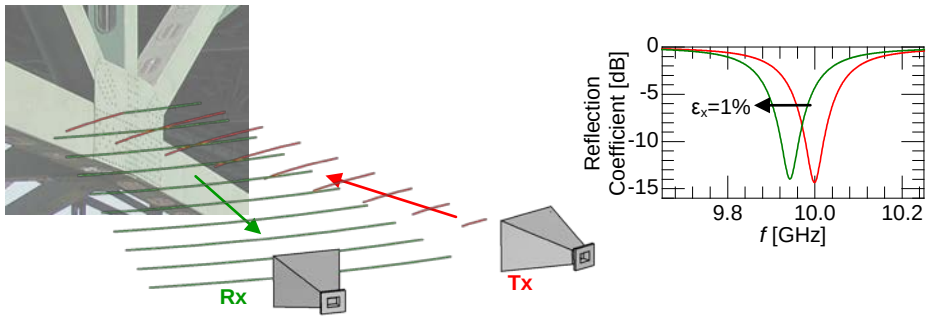

FIG 2. Illumination of FSS instrumented structure to obtain reflection coefficient and measure strain.

Based on the preceding discussion, there is a compelling case for an FSS sensing solution in the microwave, patternable using thick-film technology, and either surface mounted or embedded into the structure. Figure 1 shows a conceptual illustration of this approach. In the figure a bridge is illuminated with a beam of microwave energy. The incident beam has a broad spectrum. The structure contains a FSS which selectively absorbs, transmits, or reflects portions of the incident wave in a way that encodes structural health information into the response. A second antenna receives the energy which has interacted with the FSS and is able to translate the spectral response to the parameter of interest. The interrogation region is determined by the intersection of the beams from the two antennas.

This approach combines aspects of both global- and local- based SHM methods. The entire system can be screened for damage or parameters indicating unacceptable levels of strain, temperature, etc. from a comfortable standoff distance. If warranted, critical areas of the structure can be further interrogated by scanning a focused beam over the structure to map the parameter of interest. Similarly, metrological information about these parameters can be quantitatively determined during manufacturing or during the in-service life of the structure.

2.0 Design of FSS Strain Sensor

To illustrate the potential of the FSS technique as an SHM tool, we designed an FSS employing a tripole/anchor element to operate in the X-band (8–12 GHz). This work was presented at the IEEE Antennas and Propagation conference [17]. The X-band represents a good compromise in terms of spatial resolution, manufacturability (given the dimensions and spacing of the FSS elements), field penetration, and equipment cost. The unit cell geometry is shown in Fig. 3 along with the entire FSS under bistatic interrogation (meaning different antennas are used to transmit and receive). The interrogating beam is incident at an angle, θ, (measured from the surface normal) and has electric field polarized in the x- or y-direction (shown as $E_{i,x}$ and $E_{i,y}$ respectively, in Fig. 3). The resulting reflected signal is shown as $E_{r,x}$ and $E_{r,y}$.

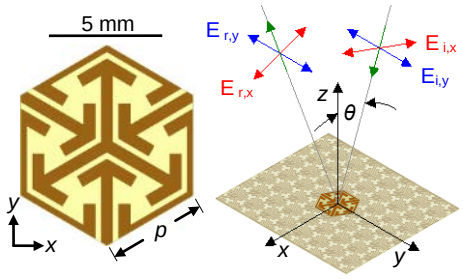

FIG 3: FSS design on 0.127 mm thick RT/Duroid 5880 with ground plane

An advantage of tripole-based FSS sensors is the ability to densely pack the elements using a hexagonal close-packed arrangement. The periodicity, *p*, of our design is 4.35 mm. The minimum spacing between the elements is 254 μm (0.010 in.) which facilitates low-cost manufacturing using conventional thick-film processing. The substrate for the design is 0.127 mm (0.005 in.) thick Rogers RT/Duroid 5880 backed by a copper ground plane. This is a commercially available low-loss laminate (relative permittivity of 2.20 and loss tangent of 0.0004) and is thin enough to be flexible and conformed to curved geometry. Such a design will be suitable for bonding to the surface of an existing structure, similar to a conventional strain gauge. In this design there is no superstrate, but in practice the FSS would be protected by a thin dielectric coating to prevent oxidation of and damage to the metallic traces.

This FSS was designed to be a resonant absorber, meaning incident electromagnetic energy will be reflected at off-resonant frequencies (there is no transmission due to the ground plane). ANSYS HFSS™ [18], a commercial full-wave Finite-Element Method solver, was used to simulate the electromagnetic response using a Floquet port analysis. This type of analysis models an infinite periodic array of unit cells. The complex reflection coefficient, Γ (the ratio of the reflected signal to the incident interrogating signal: $E_r = \Gamma\ E_i$) was simulated for planewave illumination under different angles of incidence. Both transverse electric (TE) and transverse magnetic (TM) polarizations are resolved. These correspond to *x*- and *y*-polarizations, respectively (as is illustrated above in Fig. 3). The complex reflection properties (as a function of frequency) forming the FSS signature are shown in Fig. 4 for different incident angles. As mentioned above, the periodicity is less than $0.3\lambda_0$ at the design frequency which cuts off diffraction effects, thereby reducing the dependency on the FSS signature to incident angle. While the magnitude of the FSS signature at resonance exhibits some variation as the incident angle changes, the frequency of the resonant peak shows only a minimal shift. Similar trends are

evident in the phase of the FSS signature. This insensitivity to incident angle is important for applications where normal incidence may not be ensured such as the inspection of large or curved structures.

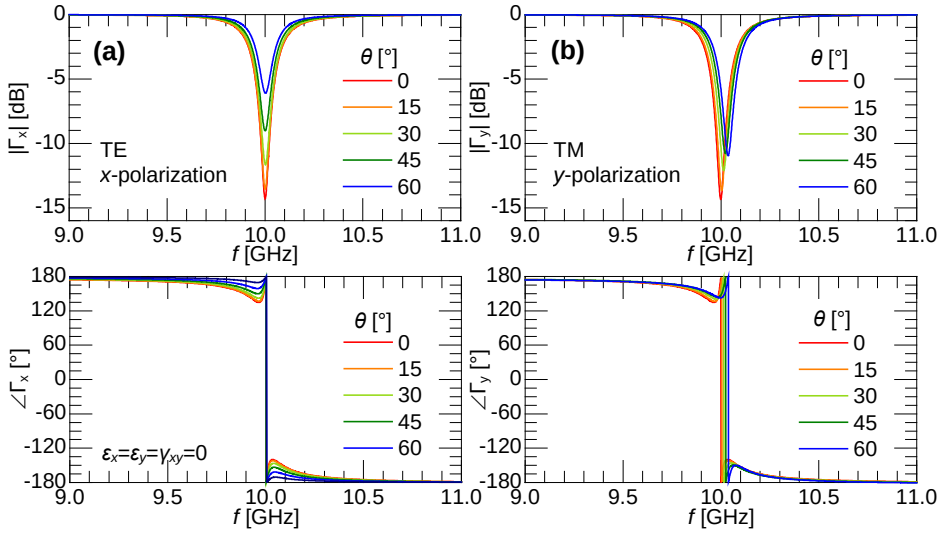

FIG 4: FSS signature for (a) *x*-polarized (TE) and (b) *y*-polarized (TM) illumination

A basic step in our approach is identifying how a change in the environment, such as strain, affects the unit cell. In the case of small strains, the geometry will be deformed according to the following transformation shown in Eq. (1) which maps original coordinates (x_0,y_0) of the FSS unit cell to the deformed position (x,y):

$$\begin{bmatrix} (1+\varepsilon_x) & \gamma_{xy} \\ \gamma_{yx} & (1+\varepsilon_y) \end{bmatrix} \begin{bmatrix} x_0 \\ y_0 \end{bmatrix} = \begin{bmatrix} x \\ y \end{bmatrix} \tag{1}$$

where ε_x is the strain in the x-direction, ε_y is the strain in the y-direction, and γ_{xy} and γ_{yx} are the shear strains. As shown in Figs. 4 and 5, prior to applying a strain, the FSS signature is insensitive to the polarization of a normally incident beam because of symmetry of the tripole/anchor. However, the resonant frequency shifts in proportion to the strain. The shift is more pronounced when the interrogating signal and reflection are polarized in the direction of strain. Figure 5 shows the effect of deforming the FSS by ε = -0.04 to 0.04 in the x and y-directions.

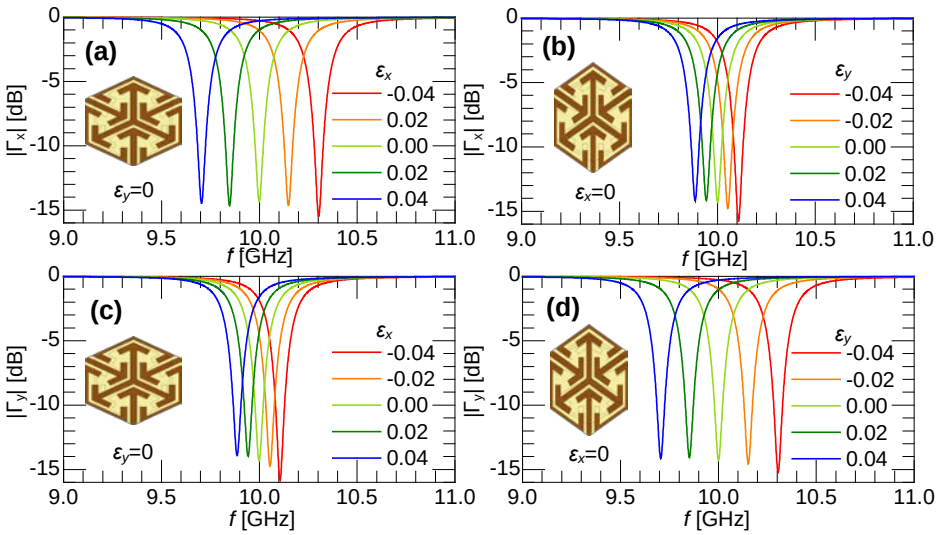

FIG 5: Magnitude of the FSS signature corresponding to strain for (a) *x* illumination under *x* strain, (b) *x* illumination under *y* strain, (c) *y* illumination under *x* strain, and (d) *y* illumination under *y* strain.

To characterize the sensitivity of the FSS signature, we simulated 225 different normal plane strain combinations in HFSS (ranging from ε = -0.07 to 0.07 in both the *x*- and *y*-directions). A Lorentzian lineshape was used to fit to each absorption spectra ($1-\Gamma^2$) to resolve the resonant frequency, f_0, and quality factor, Q, for both polarizations under normal incidence. As shown in Fig. 5, the quality factor does not change significantly. However, the shift in resonant frequency is highly linear over this range of strains. Figure 6 shows the resonant frequency as a function of ε_x and ε_y. The linearity is important as it simplifies the determination of strain on the FSS sensor. A least squares fit of the 225 resonant frequencies gives:

$$\begin{bmatrix} -0.75 & -0.28 \\ -0.28 & -0.75 \end{bmatrix} \begin{bmatrix} \varepsilon_x \\ \varepsilon_y \end{bmatrix} = \begin{bmatrix} \Delta f_{0,x} / f_0 \\ \Delta f_{0,y} / f_0 \end{bmatrix} \tag{2}$$

where $\Delta f_{0,x}$ and $\Delta f_{0,y}$ are the shifts in resonant frequency under the *x*- and *y*-polarizations, respectively, and f_0 is the original (unstrained) resonant frequency (10 GHz for this design). The FSS has only a minimal sensitivity to normal strains in the *z*-direction: $\Delta f_{0,z}/f_0/\varepsilon_z$ = 0.025. Thus, by taking two cross-polarized measurements, the normal plane strains in both directions can be determined.

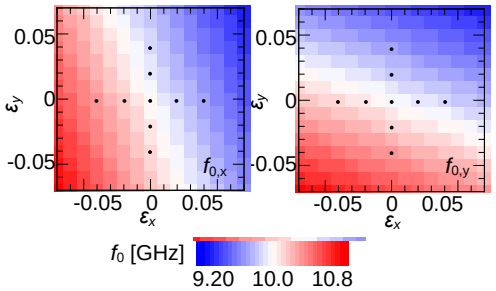

FIG 6: Simulated response of FSS under plane strain (dots indicate signatures plotted in Fig. 5).

When the thin FSS is bonded to a material with Poisson's ratio, *v*, the sensitivity to the resonant frequency can be combined to give a single axis gauge factor (GF) for this sensor design of:

$$GF = \frac{\Delta f_0 / f_0}{\varepsilon} = -0.754 + 0.253\nu \tag{3}$$

For $\nu = 0.3$, we would expect a shift of -6.77 MHz for $\varepsilon = 0.001$, and for a resolution of 100 kHz (achievable with a commercial spectrum analyzer) the strain may be resolved to better than 15×10^{-6}. Table 1 compares this design to other results from literature. It is worth noting that the designs from Malik [8-10] are split-ring resonators and only detect strain in one direction. Also, none of these structures are designed to be measured in reflection which requires that the structure be transmissive. While the structure from Jang et al. has the highest gauge factor, the elements in their work are spaced much wider their design will be subject to angular dispersion and must be measured at normal incidence.

Reference	**f_0 [GHz]**	**Sensitivity [GHz]**	**Gage Factor**
Malik et al. [10] derlin	12.7	2.22	0.175
Malik et al. [9] Si	12.8	2.30	0.180
Malik et al. [10] Si	12.8	2.35	0.184
Malik et al. [10] polyamide	12.7	3.22	0.254
Malik et al. [8]	12.3	5.15	0.419
Arritt at al. [11]	9.33	4.13	0.443
Li et al. [13]	690	368	0.533
Jang et al. [12]	10.2	7.00	0.689
This work	**10.0**	**6.77**	**0.677**

When the FSS experiences shear strain, each element undergoes a twisting deformation, breaking the symmetry of the FSS. Figure 7a shows the magnitude of the *x*-polarized reflection coefficient under shear deformation (assuming $\gamma_{xy} = \gamma_{yx}$). As before when $\varepsilon_x = \varepsilon_y = 0$, the *x*- and *y*-polarized reflections are nearly identical. Under shear loading, the *Q*-factor is significantly reduced, and for large shear strains, the original resonant peak splits into two distinct resonances.

These effects are even more dramatic when measuring the cross-polarized signature (i.e., *x*-polarized illumination and *y*-polarized measurement or vice versa), as shown in Fig. 7b. When the shear strain is zero, the cross-polarized signature is effectively zero (<-75 dB). But, for non-zero shear strain, the reflected signal becomes elliptically polarized, with a significant magnitude (-10 dB at resonance). Since the cross-polarized response does not occur in the absence of shear strain, this technique is quite promising for detection of even very small levels of shear strain. The effects of shear strain on the signature are considerably greater than what was previously predicted for a transmission based measurement in [71].

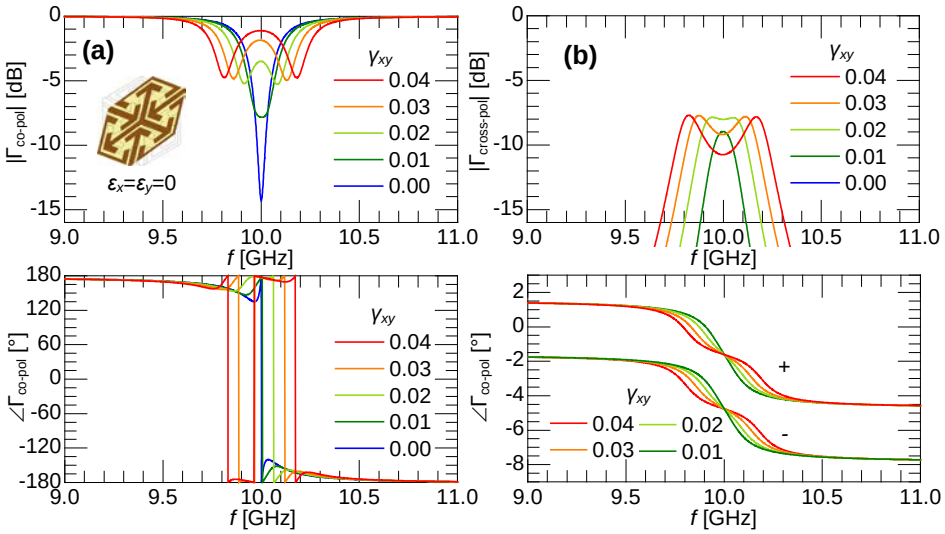

FIG 7: FSS signature under shear loading: (a) co-and (b) cross-polarized signatures.

This FSS design is also very sensitive to surface damage. Figure 8a shows a HFSS simulation of the undeformed FSS illuminated by a normally incident Gaussian beam focused to a beam width of 15 mm. Figure 8b shows the electric field normal to the surface for the case when there is a 50 μm crack in the center of the illumination beam (causing a break in a single element out of ~36 illuminated by the beam). Figure 8c shows the reflection properties of the FSS under Gaussian illumination, where a slight shift is evident in the main resonant peak (10 GHz). More importantly, an additional resonance is evident near 11 GHz, due to the response of the damaged element. These results indicate the potential for detecting this and other damage mechanisms (e.g., delamination of composite layers) which are expected to dramatically affect the FSS signature.

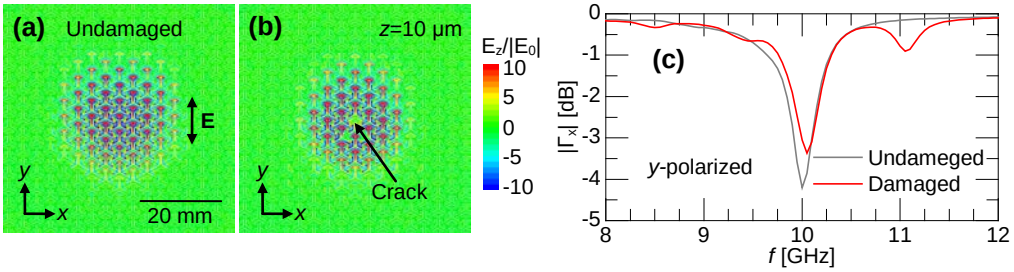

FIG 8: Normal component of electric field 10 μm above the surface for (a) undamaged FSS, (b) one of the elements with 50 μm crack, and (c) comparison of FSS signature

Figure 8 also illustrates truncation effects (i.e., the difference between the ideal response of an infinite FSS and a finite FSS). Truncation effects are generally a concern when a substantial portion of the FSS signature comes from elements on the edge of the FSS. The simulations in Figs. 4-7 considered an infinite FSS under uniform planewave illumination. In this case, since the interrogating beam has a finite beamwidth, truncation effects lead to a reduction in the magnitude of the FSS signature as compared to the ideal planewave response (Figs 4-7). If a wider beam is used, the response will converge back to the planewave (Floquet) solution. Truncation effects from a finite beamwidth lead to a potential tradeoff between spatial resolution and strain resolution. While this may require additional calibration for strain detection, the signature from a truncated FSS will still be very sensitive to damage.

3.0 Fabrication

One of the advantages of the FSS is its simplicity for fabrication. The design presented in the previous section consists only of metal patterns (no dielectrics or semiconductors). Ideally, the conductivity of the metal should be as high as possible. We explored three fabrication methods consistent with mass manufacturing: air-spray/stencil, screen-printing, and etching. The air spray/stencil and screen-printing techniques are additive approaches and are more compatible with embedding sensors within composites or other structures. Although not explored, direct-write approaches such as aerosol jet printing could also be used. Etching is a standard approach for fabricating Printed Circuit Boards (PCB). It is not compatible with printing the FSS inside a structure; however, it is valid for surface mounted sensors.

The challenge proves to be creating sufficiently high conductivity in the metallic traces without damaging the underline substrate. High conductivity is required for the FSS pattern because resistive losses in the conductive pattern lead to a much broader resonant peak. This reduces the frequency shift and will make it difficult to identify the true peak absorptance experimentally. At the conclusion of the project we are still refining the additive processes; however, the etching process was successful and created functional prototypes. It should be noted that more expensive pastes are available with low temperature curing procedures and high conductivity.

3.1 Stencil and Air-spray

One of the simplest approaches is to use a stencil to pattern the conductive pattern on the substrate. Ink can be deposited via spray with an air-brush or brushed on. A key advantage of the stencil based approach is it can accommodate singly curved preexisting geometries as illustrated in Fig. 9.

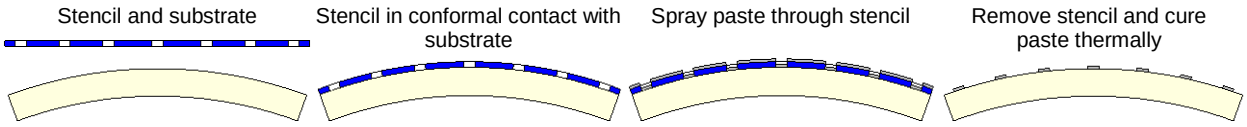

FIG 9: Air-spray/stencil patterning process on curved substrate

We purchased a spring steel stencil with the geometry presented in Fig. 3 from Thin-Metal Parts (Colorado Springs, CO). Photolithography was used to pattern photoresist and etched apertures in the metal. A photograph of the stencil is shown in Fig. 10. The majority of the stencil consists of the tripole pattern. There are also simple wire patterns at the base of the stencil for testing the DC conductivity of deposited material. The thickness of the spring steel is 0.01". A magnet was used to draw the stencil into close contact during deposition. This is necessary because a gap between the stencil and substrate causes the pattern to spread. Heraeus 1668, an air-dry silver paste (68% silver by weight) was sprayed through the stencil onto various substrates. An air-brush was used to spray the paste through the stencil. Care was taken to maintain a constant distance between spray head and the stencil. We experimented with different substrates including Kapton, Duroid and paper. Results are shown for the Duroid sample in Fig. 11. This approach is successful at patterning the tripole pattern although there are some issues with the definition at the sharp points in the array. These issues could be resolved with further process refinement.

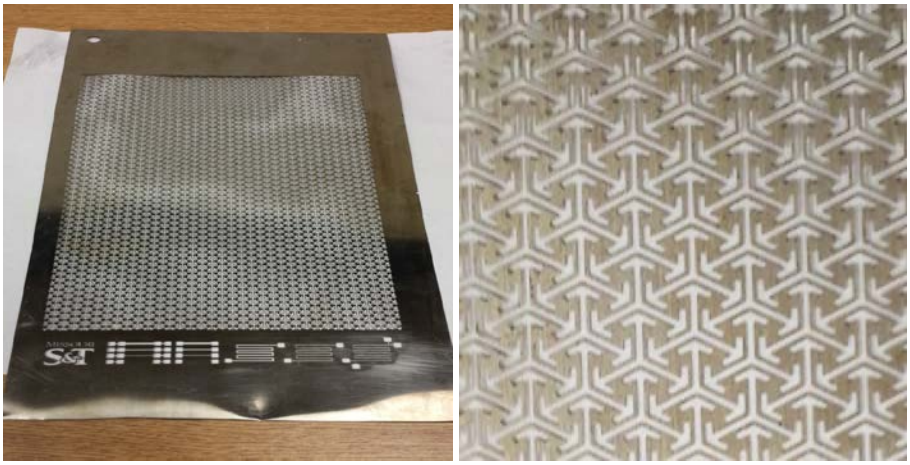

FIG 10: Photograph of stencil used with air-brush.

FIG 11: Results of patterning with stencil and air-brush on Duroid

After patterning the substrate was cured using a hot-plate 100°C. This drives off the organic solvents in the paste and increases the conductivity. Unfortunately the conductivity of the air-dry pastes is insufficient to achieve the sharp resonance in the FSS signature. Other pastes are available with higher conductivity and depending on the application air-brush patterning should be viable for depositing FSS onto/into structures [91].

3.2 Screen Printing

The next process we considered was screen printing. This approach is widely used for patterning high quality microelectronics in the Low-Temperature Co-Fired Ceramics (LTCC) process as well as for depositing the front electrodes on solar-cells [16]. It is attractive for depositing FSS

for strain sensors for several reasons; (a) screens can be easily and inexpensively prepared or purchased, (b) loops and other geometry that cannot be patterned with stencils can be patterned with screens. This process has been demonstrated for patterning metasurfaces in structural composites by Mark Mirotznik's group at the University of Delaware [19]. E. Kinzel visited their lab. While screen printing is generally used with planar substrates, it can be applied to the fiber sheets which can than be included in the composite layup. This permits 3D structural parts to be formed with 2D patterning.

We purchased a screen printing kit and used this to learn the process. The entire fabrication can be done in-house but we are still in the process of refining the parameters to produce quality prints. The process consists of coating a screen with light sensitive emulsion. The emulsion closes the pores in the screen. A positive tone mask is used to expose the emulsion in selected areas. The exposed emulsion is removed with a high pressure water jet and the pores in the screen are open for paste to pass through them. The screen is than positioned above the substrate and ink is forced through the open pores with a squeegee. There is near-contact between the screen and the substrate and parameters such as the snap-off distance, squeegee angle and ink viscosity are adjustable. Figure 12 shows some of our preliminary efforts with Methode 6105 pastes on FR4 (a standard PCB substrate). At the time of the report we are still working on patterning DC strain gauges with screen printing. Following surface patterning we will work on duplicating the Mirotznik groups work embedding them in structural composites.

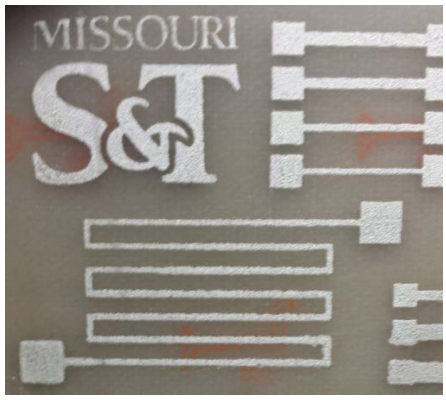

FIG 12: Results of patterning with screen-printing on FR4.

3.3 Etching

The third fabrication approach we used is etching. This is a very well established approach for PCB fabrication. We purchased negative tone masks from Fine Line Imaging (Colorado Springs, CO). These have better resolution than what could be produced using a laser printer. We shipped the masks to a colleague, H. Sigmarsson at the University of Oklahoma. He laminated a dry-film photoresist to one side of a double sided copper cladded 0.005" thick Duroid substrate. Following this step he patterned the photoresist via photolithography. Unexposed regions of the photoresist are dissolved which opens up bare copper to an etchant. Figure 13 shows a photograph of the final etched FSS.

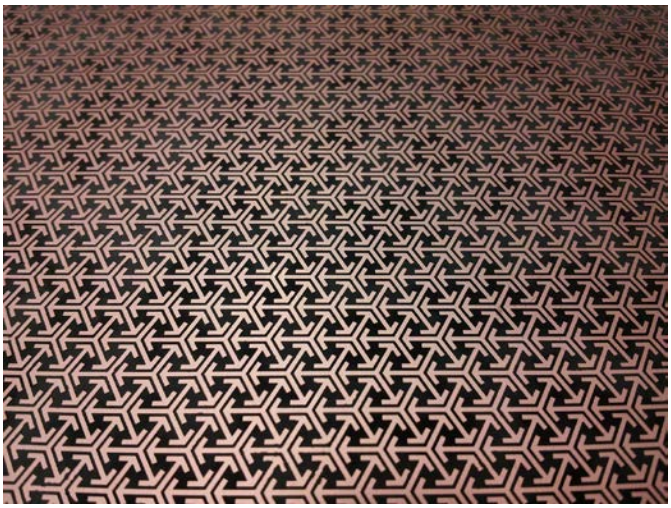

FIG 13: Etched FSS pattern on Duroid.

Besides being well established for low temperature substrates, the etching procedure has the principle advantage that the copper traces have bulk electrical conductivity without the need for high processing temperatures. The 0.005" thick Duroid is conformal and the design presented in Section 2 could be refined for Kapton or lower cost substrates. This process can be scaled up for reel-to-reel processing and create low-cost surface mounted strain gauges.

4.0 Testing

In order to validate the simulated performance of the FSS we conducted initial testing on the etched device shown in Fig. 13. Ideally, this would take place in-situ to resolve the strain/stress on a structural component during loaded. This was not feasible under the scope of the project. Instead, co-PI Donnell measured the response of the FSS using a small anechoic chamber setup. After initial measurement the FSS was plastically deformed using a Universal Testing Machine (UTM). The strain in the FSS was measured using an extensometer during testing and by measuring changes in the element spacing with a microscope. The FSS was measured again using the small anechoic chamber setup.

While still preliminary, these measurements are in general agreement with the HFSS simulation. Future work will be conducted using a free-space measurement system. This will remove some of the experimental uncertainty associated with the preliminary measurements.

4.1 Mechanical

After baseline measurements were conducted, the etched sample was mechanically strained using an Instron UTM. The sample was measured 9"×6" and was subjected to tensile loading. Figure 14 shows a photograph of the FSS loaded into the UTM. Aluminum taps were attached to the top and bottom to match the fixturing for the UTM and create as uniform strain on the surface of the FSS as possible.

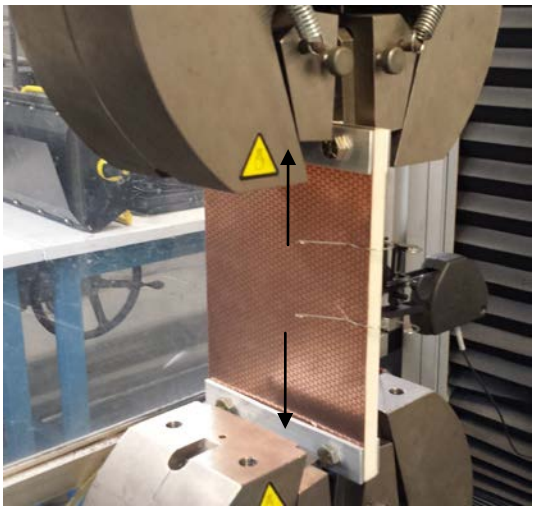

FIG. 14: FSS loaded in UTM during tensile loading

The FSS strained by 0.98% when leaded by 170 lbf. This was corroborated by measuring the average distance between elements using a microscope with the original element spacing taken from the nominal dimension of the FSS. The microscope measurement gave the strain along the direction of loading as 1.09%. The extension/load curve from the UTM experiment showed some slip during the initial loading of the sample and the intra-element spacing measurement is likely to be more accurate.

Because of buckling of the initial test specimen, two additional FSS were epoxyed to ABS plastic pieces. These were also strained in tension and shear (shown in Fig. 15.). These specimens will be tested when co-PI Donnell's student returns from an internship.

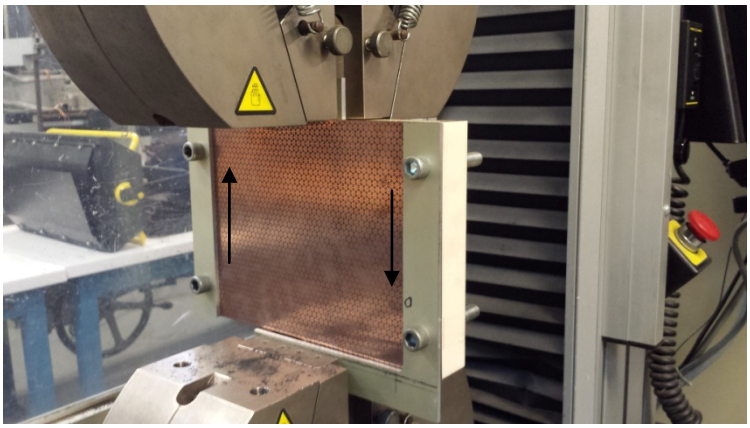

FIG. 15: FSS loaded in UTM during shear loading

4.2 Electromagnetic

The FSS sample was measured using a small anechoic chamber setup in co-PI Donnell's laboratory. In this setup the sample is illuminated with a horn antenna from varying distances. A horn antenna is used to receive radiation reflected from the FSS. Both horn antennas are connected via co-ax cables to the ports of a network analyzer. This allows the transmission from one antenna to the other antenna to be measured as a function of frequency. Calibration of the

network analyzer poses a significant challenge as energy emitted from the first antenna can be scattered from surfaces other than the FSS and still be received by the second antenna. For this reason the sample and the antennas are placed in a box with RAM (Radar Absorbing Material). While not eliminating all reflections and scatter the small anechoic chamber does help to minimize noise. The network analyzer was calibrated to a metal reflective surface at the same distance from the antennas as the FSS in the experiment. Figure 16 shows the experimentally measured transmission coefficient (nominally corresponding to the reflection coefficient from one antenna to the other) which was measured for the FSS in Fig. 13.

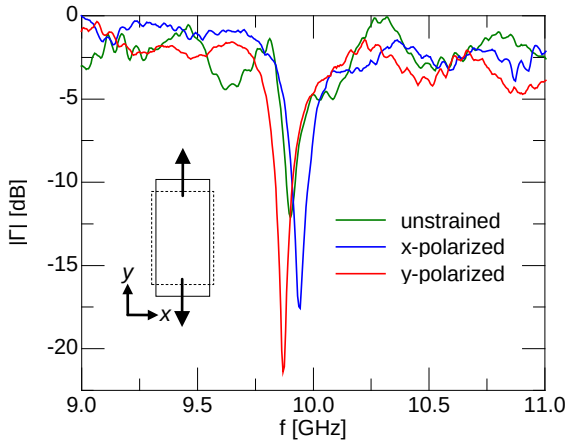

FIG. 15: Preliminary results of microwave testing of unstrained and strained FSS.

Figure 13 shows that the resonant frequency is slightly lower than was expected from the simulation (see Fig. 5). This can be explained because the FSS was slightly over etched, resulting in a larger gap between adjacent elements and hence lower capacitive loading. The experimental result shows that the after loading the absorption peak shifted -0.29 GHz. The absorption peak shifted +0.023 GHz when the radiation is polarized perpendicular to the direction of axial loading.

These results agree qualitatively with the simulation results. Future testing using a free-space measurement setup will be required because of the difficulty in calibrating the small anechoic chamber equipment.

5.0 Conclusion

Overall this project has demonstrated the potential for using FSS for structural health monitoring. We reviewed literature on SHM techniques and sensing methods. This included identifying a small handful of other research groups who have proposed similar concepts in the past 5 years. We designed a new type of FSS sensor with the capability of resolving plane strain including shear. With the proper microwave test equipment we have the potential of monitoring in-plane strain at the sub-100 microstrain level. We investigated different fabrication methods. Ultimately conventional PCB fabrication including etching may be best for this type of sensing application. Finally we conducted initial testing, with more rigorous testing ongoing over the summer.

5.1 Future Work

Applying FSS as a remote sensing technique is new and there is still considerable work to be done. Much more rigorous microwave testing is required to determine the resolution of the sensor; both in terms of strain resolution and in-terms of spatial resolution. While the preliminary testing work done in this proposal supports the simulation results. Much more rigorous free-space measurements are required. We are hopeful these measurements can be made at AFRL before the end of the summer. Along these lines, any successful sensing system will require new approaches to measuring these sensors. Much of this can draw from radar techniques but some will be unique to applying FSS to engineering structures. For instance, accurately locating damage in a large structure, determining the sensitivity to features such as cracks, avoiding false positives etc.

On the sensor design side there is still considerable work to be done on increasing the gauge factor. While the design in this report is competitive with literature (excluding the design which is not subject to gross angle of incidence sensitivity), work needs to be done to establish what is the maximum sensitivity for an FSS sensor. This should be done on a theoretical as well as experimental basis. Measuring strain is only scratching the surface of what can be measured with these sensors. Work should be conducted to design sensors for monitoring pressure, temperature, chemical species, etc..

Finally, more work needs to be done on the fabrication of these sensors. Much of our original work was motivated by the possibility of including these sensors in composites. However, most advanced structural composites are not transparent to microwaves. There is potential for embedding in plastics, cement, and glass-fiber/epoxy composites. Surface mounted sensors do show potential for systems that cannot be penetrated by radiation. Standard PCB approaches are acceptable for the surface mounted sensor. More work is required to refine the additive techniques for manufacturing embedded systems.

5.2 Project Deliverables

The project deliverables (outside of the Final Report) for this award focused on publications and creating a prototype. We have generated a design and several prototypes. The design itself has recently been presented at the 2014 IEEE Antennas and Propagation Conference [17]. After more rigorous free-space testing is completed this paper will be expanded for a journal publication.

Related to this, a full length proposal was submitted to NSF. In addition, E. Kinzel was awarded a Summer Faculty Fellowship at the Air Force Research Laboratory on the basis of this work.

5.3 Publications and Student Support

The following publication resulted from this Grant:

1. E. Kinzel, “Design of a Frequency-Selective Surface Strain Sensor”, *Proceedings of the IEEE Antennas and Propagation Conference*, July 6-11th, Memphis TN.

The following students have been supported on this Grant:

1. Mr. Harshvardhan Sahu, Mechanical and Aerospace Engineering, MS, Missouri University of Science and Technology
2. Mr. Arvindvivek Ravichandran, Mechanical and Aerospace Engineering, MS, Missouri University of Science and Technology

6.0 References

1. C. Farrar and K. Worden, "An introduction to structural health monitoring," *Phil. Trans. R. Soc. A*, vol. 365, pp. 303-315, Dec. 2006.
2. J. P. Lynch and K. J. Loh, "A Summary Review of Wireless Sensors and Sensor Networks for Structural Health Monitoring," Shock and Vibration Digest, vol. 38, no. 2, pp. 91-128, Mar. 2006.
3. G. Park T. Rosing, M. D. Todd, C. R. Farrar, and W. Hodgkiss, "Energy Harvesting for Structural Health Monitoring Sensor Networks," J. Infrastructure Syst., vol. 14, pp. 64-79, 2008.
4. S. E. Watkins, G. W. Sanders, F. Akhavan, and K. Chandrashekhara, "Modal analysis using fiber optic sensors and neural networks for prediction of composite beam delamination," Smart Materials and Structures vol. 11, no. 4, pp. 489-495, 2002.
5. B.A. Munk, Frequency Selective Surfaces, Theory and Design, New York: Wiley-Interscience, 2000.
6. B.A. Munk, Metamaterials, Critique and Alternatives, Hoboken, John Wiley & Sons, Inc. 2009.
7. D. R. Smith, S. Schultz, P. Markoš, and C. M. Soukoulis, "Determination of effective permittivity and permeability of metamaterials from reflection and transmission coefficients," Phys. Rev. B, vol. 65, no. 19, 195104, 2002.
8. R. Melik et al. "Metamaterial-based wireless strain sensors," Appl. Phys. Lett., vol. 95, pp. 011106, 2009.
9. R. Melik et al. "Flexible metamaterials for wireless strain sensing," Appl. Phys. Lett., vol. 95, pp. 181105, 2009.
10. R. Melik et al. "Metamaterial based telemetric strain sensing in different materials." Optics Exp., vol. 18, no. 5, 2010.
11. B. Arritt, B. Adomanis, T. Khraishi, and D. Smith, "Parameteric analysis of the strain-dependent behavior of a metamaterials electric resonator," Appl. Phys. Lett., vol. 97, pp. 191907, 2010.
12. S.-D. Jang, B.-W. Kang, and Jaehwan Kim. "Frequency selective surface based passive wireless sensor for structural health monitoring." Smart Materials and Structures , vol. 22 no. 2, pp. 025002, 2013.

13. J Li et al., "Flexible terahertz metamaterials for dual-axis strain sensing." Opt. Lett., vol. 38, no. 12, pp. 2104-2106, 2013.

14. Ye, Yong-Hong, D-Y. Jeong and Q. M. Zhang. "Fabrication of strain tunable infrared frequency selective surfaces on electrostrictive poly (vinylidene fluoride–trifluoroethylene) copolymer films using a stencil mask method." Appl. Phys. Lett., vol. 85, no. 4, pp. 654-656, 2004.

15. I. M. Pryce, et al. "Highly strained compliant optical metamaterials with large frequency tunability." Nano Lett., vol. 10, no. 10, pp. 4222-4227, 2010.

16. J. J. Licari and L. R. Enlow, “Hybrid Microcircuit Technology Handbook, Materials, Processes, Design and Production, 2nd ed. Westwood, NJ: Noyes Publications, 1998.

17. E. Kinzel, “Design of a Frequency Selective Surface Strain Sensor,” Proceedings of the IEEE Antennas and Propagation Conference, Memphis TN, July 2014.

18. HFSS Version 15.0, ANSYS Inc. Cannonsburg PA.

19. M. S. Mirotznik, S. Yarlagadda, R. McCauley and Peter Pa, “Broadband Electromagnetic Modeling of Woven Fabric Composites,” IEEE Trans. Microw. Theory Tech., vol. 60, no. 1, pp. 158-169, Jan. 2012.